Research Square

Preprints are preliminary reports that have not undergone peer review.
They should not be considered conclusive, used to inform clinical practice,
or referenced by the media as validated information.

ASS1 deficiency promotes ferroptosis vulnerability in dopaminergic neurons in Parkinson's disease

Linpei Zhuo
The Second Affiliated Hospital of Wenzhou Medical University
Zongtang Xu
The Second Affiliated Hospital of Wenzhou Medical University
Conghui Dai
Wenzhou Medical University
Yao Yang
Wenzhou Medical University
Kun Xiang
The Second Affiliated Hospital of Wenzhou Medical University
Qiyao Li
The Second Affiliated Hospital of Wenzhou Medical University
Zheyu Fang
The Second Affiliated Hospital of Wenzhou Medical University
Dong Chen
Wenzhou Seventh People's Hospital of Wenzhou Medical University
Jiaming Liu
wzjiaming_liu@163.com
Wenzhou Medical University
Jing Sun
The Second Affiliated Hospital of Wenzhou Medical University

Article

Keywords: Parkinson's disease, ASS1, dopaminergic neurons, amino acid metabolism, ferroptosis, virtual screening

Posted Date: May 27th, 2026

DOI: https://doi.org/10.21203/rs.3.rs-9722320/v1

License: This work is licensed under a Creative Commons Attribution 4.0 International License.
Read Full License

Additional Declarations: No competing interests reported.

Abstract

Parkinson's disease (PD) is characterized by progressive degeneration of dopaminergic neurons in the substantia nigra. However, the metabolic mechanisms linking neuronal vulnerability to ferroptosis remain poorly understood. To address this question, we integrated single-nucleus and bulk RNA sequencing datasets from human substantia nigra to characterize cell-type-specific transcriptional alterations in PD. Integrative transcriptomic analyses including Weighted gene co-expression network analysis, pathway enrichment analysis, and correlation analysis, were further validated using MPTP-induced mouse models and MPP^+-treated SH-SY5Y cells combined with gene silencing and ferroptosis-related assays. In addition, structure-based virtual screening of 12,316 DrugBank compounds was conducted to identify potential modulators of key metabolic targets. We found that dopaminergic neurons exhibited preferential activation of ferroptosis signatures accompanied by marked dysregulation of amino acid metabolic pathways. Among metabolism-related genes, argininosuccinate synthase 1 (ASS1) emerged as a key candidate with favorable diagnostic performance and significant positive correlations with ferroptosis-suppressive genes, including GPX4 and GSS. In MPTP-induced mice, ASS1 expression was significantly reduced in the substantia nigra and dopaminergic neurons. Consistently, ASS1 silencing in MPP^+-treated SH-SY5Y cells further decreased cell viability and reduced TH and GPX4 expression, while markedly increasing lipid peroxidation, indicating enhanced ferroptosis susceptibility. Virtual screening further identified several therapeutically relevant compounds with favorable predicted binding to an ASS1 docking pocket. Collectively, these findings identify ASS1-associated amino acid metabolic impairment as a prominent feature of dopaminergic ferroptosis in PD and highlight ASS1 as a potential therapeutic target for neuroprotective intervention.

1. Introduction

Parkinson's disease (PD) is a common and progressive neurodegenerative disorder characterized clinically by bradykinesia, rigidity, resting tremor, and postural instability. Although the etiology of PD is multifactorial and incompletely understood, the selective degeneration of dopaminergic neurons in the substantia nigra pars compacta (SNpc) and the consequent depletion of striatal dopamine are widely recognized as the central neuropathological features underlying motor symptom manifestation.

Accumulating evidence indicates that dopaminergic neuron loss in PD arises from the convergence of multiple pathogenic mechanisms, including mitochondrial dysfunction, oxidative stress, and dysregulated iron homeostasis [1–3]. These processes collectively impose extraordinary metabolic demands on dopaminergic neurons[4–6], which are intrinsically vulnerable due to their extensive axonal arborization, autonomous pacemaking activity, and high bioenergetic requirements [7]. Consequently, increasing attention has been directed toward metabolic perturbations as upstream drivers of neuronal vulnerability in PD.

Recent advances in high-throughput transcriptomic and metabolomic profiling have revealed widespread metabolic alterations in PD-affected brain regions [8] [9]. Among these, amino acid metabolism has

emerged as a recurrently dysregulated pathway. Amino acids play indispensable roles in redox regulation, mitochondrial function, and cellular stress responses [10]. Disruption of these pathways may therefore compromise neuronal homeostasis and sensitize cells to regulated forms of death such as ferroptosis, which has been increasingly implicated in PD pathophysiology [11, 12] [13].

Arginine metabolism represents a particularly compelling axis in this context. Arginine serves as a precursor for nitric oxide synthesis, polyamine production, and multiple downstream metabolites essential for redox balance and cellular survival [14, 15]. Argininosuccinate synthase 1 (ASS1), the rate-limiting enzyme of endogenous arginine biosynthesis, occupies a central position in nitrogen metabolism by catalyzing the conversion of citrulline and aspartate to argininosuccinate [16]. Altered ASS1 expression has been reported in diverse pathological conditions and is frequently associated with increased susceptibility to oxidative damage and regulated cell death[17, 18]. Despite its metabolic importance, the role of ASS1 in PD and dopaminergic neuron vulnerability has not been systematically explored. In addition, current pharmacological treatments effectively alleviate symptoms but do not prevent continued neuronal degeneration, highlighting a critical gap in disease-modifying therapeutic strategies.

In this study, we integrated single-nucleus and bulk transcriptomic data to characterize amino acid metabolic dysregulation in Parkinson's disease through irGSEA, hdWGCNA, differential gene expression analysis, multiple pathway enrichment analyses, and correlation analyses at both single-nucleus and bulk transcriptomic levels. Through cell-based and animal model experiments, we further validated that downregulation of ASS1 exacerbates ferroptosis-related injury in dopaminergic neurons. Additionally, virtual screening was performed to identify compounds with predicted binding affinity to the key metabolic gene ASS1. In conclusion, by integrating multi-omics analysis with experimental validation, we have established a framework that links ASS1 downregulation to enhanced ferroptosis susceptibility in dopaminergic neurons, thereby nominating ASS1 as a promising therapeutic target for PD.

2. Results

2.1 Single-nucleus integration defines dopaminergic neurons as the primary carriers of Parkinson's disease–associated transcriptional programs

Single-nucleus RNA-seq data from the human substantia nigra pars compacta were first processed with standard quality-control filtering (Figure S1). After quality control, integration of the retained nuclei resolved seven major cell populations, including neurons, astrocytes, microglia, oligodendrocyte lineage cells, vascular cells, and T cells, supported by canonical marker expression (Fig. 1A, B). The average number of nuclei per donor was comparable between early-stage and moderate PD groups, reducing the likelihood of sampling bias between disease stages (Fig. 1C).

Neuronal reclustering revealed three transcriptionally distinct subtypes: dopaminergic neurons (cluster 0), excitatory neurons (cluster 1), and inhibitory neurons (cluster 2), defined by established marker genes (Fig. 1D, E). Given that dopaminergic neurons are the primary neuronal population undergoing degeneration in PD, subsequent analyses were focused on cluster 0 to capture disease-relevant molecular alterations.

Pathway scoring using irGSEA demonstrated that PD-related Kyoto Encyclopedia of Genes and Genomes (KEGG) pathways were consistently more active in dopaminergic neurons across four independent scoring algorithms, whereas excitatory and inhibitory neurons showed substantially lower pathway activity (Fig. 1F-M). Together, these results indicate that dopaminergic neurons not only represent the major cellular population affected in PD but also harbor the most prominent PD-associated transcriptional programs, providing a rational cellular focus for downstream analyses.

2.2 Dopaminergic neurons exhibit preferential activation of ferroptosis together with broad metabolic pathway dysregulation

To identify pathways specifically enriched in dopaminergic neurons, KEGG pathway activity was ranked using four independent irGSEA scoring methods (AUCell, UCell, ssGSEA, and singscore). The top-ranked pathways based on average difference scores showed consistent enrichment patterns across methods, highlighting multiple metabolic and stress-related pathways in dopaminergic neurons (Fig. 2A). Intersection analysis revealed nine consistently enriched pathways, with ferroptosis robustly identified across all scoring methods (Fig. 2B).

Consistent with this finding, ferroptosis pathway scores were significantly higher in dopaminergic neurons (cluster 0) compared with excitatory (cluster 1) and inhibitory neurons (cluster 2) across all four scoring methods (Fig. 2C–G), indicating preferential activation of ferroptosis in this neuronal subtype.

Analysis of neuronal composition revealed a reduced proportion of dopaminergic neurons in higher Braak stages (III–IV) compared with lower stages (I–II) (Fig. 2H), consistent with progressive dopaminergic neuron loss. UMAP visualization further separated dopaminergic and non-dopaminergic neuronal populations, providing a basis for downstream classification and analysis (Fig. 2I).

Functional categorization of significantly altered KEGG pathways demonstrated that metabolism represented the most enriched category in dopaminergic neurons, with amino acid metabolism comprising the largest subcategory (Fig. 2J). These results suggest that ferroptosis activation in dopaminergic neurons occurs in the context of extensive metabolic reprogramming, particularly involving amino acid pathways.

2.3 Co-expression network analysis identifies a dopaminergic neuron–specific module enriched for Parkinson's disease and ferroptosis-related pathways

To determine whether PD-associated transcriptional alterations in dopaminergic neurons reflect coordinated gene programs rather than isolated gene changes, we performed hdWGCNA on the neuronal subset. This analysis identified three robust gene modules under a signed network with optimal soft-threshold power selection (Fig. 3A-E).

Module 1 was enriched for Parkinson's disease, ferroptosis, necroptosis and synaptic-related pathways, whereas Modules 2 and 3 were associated predominantly with excitatory and inhibitory neuronal functions, respectively (Fig. 3F). Visualization of the top hub genes per module further highlighted the distinct molecular composition of each module (Fig. 3G).

Module eigengene and hub score projections demonstrated that Module 1 activity was strongly concentrated in dopaminergic neurons, confirming it as a dopaminergic neuron–specific co-expression module (Fig. 3H-K). These findings indicate that PD-associated cell death and metabolic pathways are embedded within a coordinated transcriptional network specific to dopaminergic neurons.

2.4 Integrated bulk transcriptomics reveals coordinated suppression of amino acid metabolic pathways in Parkinson's disease

To assess whether dopaminergic neuron–associated transcriptional changes are reflected at the tissue level, we analyzed bulk RNA-seq data from PD and control substantia nigra. Differential expression analysis detected 246 upregulated genes and 1, 204 downregulated genes between PD and control substantia nigra samples (Fig. 4A).

Intersection of bulk differentially expressed genes with neuronal hdWGCNA module genes yielded 707 overlapping genes (Fig. 4B), supporting concordance between single-nucleus and bulk transcriptomic level alterations. Representative overlapping genes were visualized across both datasets to illustrate consistent expression trends (Fig. 4C, F).

Gene Ontology (GO) and KEGG enrichment analyses of overlapping genes consistently highlighted amino acid metabolism–related processes (Fig. 4D, E). GSEA further demonstrated coordinated negative enrichment of five amino acid metabolic pathways in PD, among which alanine, aspartate and glutamate metabolism showed the strongest signal (Fig. 4G, H). Examination of the 14 genes within this pathway revealed an overall downward expression pattern in PD bulk tissue, with approximately half of these genes showing statistically significant reductions, including ADSL, GLS2, GAD2, ASS1, GOT1, NIT2, and ASRGL1 (Fig. 4I), indicating broad suppression of amino acid metabolic capacity in PD.

2.5 ASS1 emerges as a central metabolic gene linking dopaminergic vulnerability to inhibition of ferroptosis

To identify candidate genes linking amino acid metabolism to dopaminergic neuron vulnerability, we examined genes involved in the alanine, aspartate and glutamate metabolism pathway. Single-nucleus

transcriptomic analysis identified ten genes with prominent expression in neuronal populations (Fig. 5A). The expression patterns of these ten genes were visualized on the neuronal UMAP, illustrating their distributions across neuronal subpopulations (Figure S2). ROC analysis identified four genes with diagnostic value for distinguishing PD from control samples, including ASS1, NIT2, ASRGL1 and GOT1 (Fig. 5B-F). Notably, all four genes were significantly downregulated in PD bulk tissue compared with controls (Fig. 4I). Among them, ASS1 showed the highest AUC value (0.803), highlighting ASS1 as a metabolically relevant candidate gene in PD.

Pathway mapping confirmed that ASS1 participates not only in alanine, aspartate and glutamate metabolism but also in arginine biosynthesis and the urea cycle, underscoring its central position in nitrogen and amino acid metabolism (Fig. 5G). At the single-nucleus level, stratified analysis showed that ASS1 expression decreased from Braak I–II to Braak III–IV in both dopaminergic and non-dopaminergic neurons (Fig. 5H-J), suggesting an association with pathological severity.

Correlation analyses further revealed strong positive associations between ASS1 and key regulators that inhibit ferroptosis, including GPX4 and GSS (Fig. 5K–M). Together, these findings identify ASS1 as a metabolically relevant gene associated with dopaminergic neuron vulnerability and ferroptosis-related transcriptional signatures in PD.

2.6 ASS1 downregulation exacerbates ferroptosis and dopaminergic neuronal injury in PD models

To validate the association between ASS1 and ferroptosis in dopaminergic neuron degeneration, we performed both in vivo and in vitro experiments. In the MPTP-induced PD mouse model, qPCR analysis revealed a significant reduction in *ASS1* mRNA expression in the substantia nigra compared with controls (Fig. 6A). Consistently, western blot analysis confirmed decreased protein levels of ASS1 and TH in MPTP-treated mice (Fig. 6B–D). Immunofluorescence staining further demonstrated reduced TH-positive dopaminergic neurons accompanied by diminished ASS1 expression in the substantia nigra (Fig. 6E–G).

To investigate the functional role of ASS1 in vitro, SH-SY5Y cells were treated with MPP^+ to establish a PD-like injury model. CCK-8 assays showed a dose-dependent decrease in cell viability, and 1500 μM MPP^+ was selected for subsequent experiments as the lowest concentration inducing a significant reduction in viability (Fig. 6H). Compared with control cells, MPP^+ treatment significantly reduced cell viability, which was further exacerbated by ASS1 knockdown (Fig. 6I). Western blot analysis demonstrated that knockdown of ASS1 led to a marked reduction in TH and GPX4 protein levels, both under basal conditions and following MPP^+ exposure (Fig. 6J–M), indicating impaired dopaminergic phenotype and reduced ferroptosis resistance. Consistent with these findings, C11-BODIPY staining revealed increased lipid peroxidation in ASS1-silenced cells, particularly under MPP^+ treatment (Fig. 6N, P). In parallel, immunofluorescence staining showed a significant decrease in GPX4 signal intensity in the siASS1 + MPP^+ group (Fig. 6O, Q).

Collectively, these results demonstrate that ASS1 downregulation promotes ferroptosis-associated lipid peroxidation, reduces GPX4 expression, and exacerbates dopaminergic neuronal injury, supporting a functional role for ASS1 in regulating ferroptosis susceptibility in Parkinson's disease.

2.7 Virtual screening identifies candidate ASS1 binders with favorable predicted central nervous system properties

To explore pharmacological strategies targeting ASS1-associated metabolic vulnerability, we performed virtual screening of 12,316 DrugBank compounds against an ASS1 docking pocket defined by the LM-2I binding region [19]. This approach identified 114 ligands with favorable MM-GBSA binding energies and acceptable predicted blood–brain barrier permeability (Figure S3A).

Ten compounds were prioritized based on integrated consideration of binding strength, CNS penetration and reported safety profiles (Figure S3B), including apomorphine, S-apomorphine, propranolol, dexpropranolol, dichloroisoproterenol, tulobuterol, demexiptiline, safrazine, cloridarol, and TRANS-(1S,2S)-2-AMINO-1,2,3,4-TETRAHYDRONAPHTHALEN-1-OL (TTL). These candidates spanned several clinically relevant drug classes and all demonstrated stable binding poses within the ASS1 pocket (Figure S3C-L, Figure. S4), nominating ASS1 as a potentially druggable metabolic node warranting further experimental validation in PD models.

3. Discussion

Parkinson's disease is defined by the progressive loss of dopaminergic neurons, yet the molecular programs that couple neuronal ferroptotic vulnerability to disease progression remain incompletely understood. In this study, we addressed whether transcriptional dysregulation of amino acid metabolism contributes to dopaminergic neuron death in PD. By integrating single-nucleus transcriptomic profiling with bulk RNA-seq data, we systematically mapped cell-type–specific pathway alterations, gene co-expression modules and metabolic signatures associated with dopaminergic vulnerability. Our analyses identify coordinated activation of ferroptosis-related programs in dopaminergic neurons, accompanied by broad suppression of amino acid metabolic pathways. Within this framework, ASS1 emerged as a central metabolic gene linked to both dopaminergic degeneration and regulators of cell death inhibition. Importantly, these computational findings were further supported by in vitro and in vivo experiments demonstrating that ASS1 downregulation enhances ferroptosis-associated neuronal injury. The following discussion places these findings in the context of PD pathophysiology, examines the potential role of ASS1-mediated metabolic dysfunction in neuronal ferroptosis, and considers implications for therapeutic targeting.

Dopaminergic neurons constitute the most selectively vulnerable and functionally determinative neuronal class in PD. In alignment with neuropathological reports, our single-nucleus transcriptomic analyses demonstrated a pronounced reduction of dopaminergic neurons in PD substantia nigra, accompanied by elevated signatures of ferroptosis. Dopaminergic neuron loss is widely regarded as a core event that reflects both the onset and progression of PD, and convergent evidence has implicated

chronic neuroinflammation, mitochondrial dysfunction, and oxidative stress as major pathological pathways driving dopaminergic cell death in patients [20, 21]. Beyond cell survival deficits, we observed transcriptional enrichment of amino acid metabolic programs, reflecting a shift toward metabolic reprogramming under PD-associated stress. This pattern is consistent with prior metabolomic profiling linking PD progression to disrupted amino acid homeostasis [22–24]. Together, these observations suggest that dopaminergic neurons in PD are subjected to a combined burden of ferroptosis and metabolic imbalance.

Bulk-level enrichment analyses further reinforced this metabolic axis, revealing convergent dysregulation of amino acid pathways across GO, KEGG, and GSEA platforms, a finding that carries significant pathophysiological implications. Multiple amino acid modules displayed negative enrichment. In the top-ranked alanine, aspartate and glutamate metabolism pathway, 10 genes, namely GOT1, GOT2, ASNS, GAD2, ASRGL1, ALDH5A1, GAD1, ASS1, GLS2, and NIT2, were distinctly expressed in neuronal populations, indicating that these genes are not background signals. More importantly, it suggests that amino-acid–linked transcriptional imbalance is concentrated within neuronal compartments rather than being a generalized tissue artifact.

Among these candidates, ASS1 demonstrated the strongest diagnostic performance, with an AUC of 0.803. Integrating single-nucleus and bulk transcriptomic differential expression findings, our data indicate that reduced ASS1 expression is a defining feature of dopaminergic neurons within the PD brain. As the rate-limiting enzyme of endogenous arginine biosynthesis, ASS1 catalyzes the condensation of citrulline and aspartate to form argininosuccinate, thereby occupying a nodal biochemical position[15]. KEGG mapping further confirmed its participation not only in alanine, aspartate and glutamate metabolism but also in the urea cycle, ornithine–citrulline nitrogen transfer, and arginine biosynthesis. These convergent roles highlight ASS1 as a central metabolic node with potential relevance for PD.

Multiple lines of evidence support that arginine depletion is tightly coupled to cell death susceptibility. Reductions in intracellular arginine limit nitric oxide synthesis, disrupt mitochondrial redox balance, and precipitate ROS accumulation leading to apoptotic signaling [25]. Arginine scarcity further destabilizes dNTP equilibrium, increasing replication stress and activating p53-mediated death programs [18]. Additionally, arginine withdrawal attenuates glutamine-dependent metabolic buffering and reduces cellular capacity to withstand ferroptotic stress [17]. These findings support a potential link between dysregulated arginine metabolism and dopaminergic neuron loss in Parkinson’s disease. In this study, we identified consistent downregulation of ASS1, a key enzyme in arginine biosynthesis, in dopaminergic neurons, together with its strong association with signatures of ferroptosis-related programs. Given the central role of ASS1 in maintaining intracellular arginine pools [16], reduced ASS1 expression may contribute to altered arginine metabolism and increased susceptibility of dopaminergic neurons to ferroptosis.

In tumor systems, ASS1 loss has been exploited therapeutically to induce cell death, highlighting its regulatory influence on metabolic survival checkpoints. ASS1-deficient tumors demonstrate marked

sensitivity to arginine depletion, and ADI-PEG20 administration elicits ROS accumulation and mitochondrial dysfunction in breast cancer models [26]. In sarcomas, ASS1 deficiency renders cells susceptible to ADI-PEG20–induced necroptosis, while ASS1 silencing removes glutamine-mediated reductive carboxylation, weakening ferroptosis resistance in non-small-cell lung cancer [17, 27]. Although disease contexts differ, these findings collectively support that ASS1 loss constitutes a central metabolic trigger for susceptibility to ferroptosis. Extrapolated to PD, such data further strengthen the notion that reduced ASS1 expression may lower the threshold for dopaminergic neuronal ferroptosis under chronic stress.

Consistent with this relationship, our correlation analyses demonstrated that reduced ASS1 expression in PD dopaminergic neurons coincides with lowered expression of canonical ferroptosis-protective genes, including GPX4 and GSS[28, 29]. To further evaluate this association, we performed functional experiments and found that ASS1 silencing resulted in a significant reduction of GPX4 expression at both protein and immunofluorescence levels. In addition, ASS1 knockdown increased lipid peroxidation in SH-SY5Y cells, further indicating enhanced ferroptosis under ASS1 deficiency. In this context, ASS1 appears to act as a metabolic regulator linking amino acid metabolism to ferroptosis susceptibility.

Conversely, enhanced ASS1 expression has been shown to exert protective effects in multiple cellular systems. In human cerebral microvascular endothelial cells, ASS1 upregulation mitigates mutation-driven neurovascular impairment [30]. In diabetic endothelium, ASS1 overexpression attenuates pathological calcification, and Sirtuin-3-mediated deacetylation of ASS1 promotes arginine biosynthesis, imparting vascular protection [31]. Comparable neural relevance has been documented in zebrafish, where ASS1 deficiency impairs neuronal differentiation and constrains neural tissue expansion, suggesting auxiliary roles in neurodevelopmental maintenance [32, 33]. Together, these observations indicate that restoring or sustaining ASS1 activity may confer broad cytoprotective benefits at both vascular and neuronal levels. In this context, therapeutic strategies aimed at enhancing or stabilizing ASS1 function may hold potential for mitigating metabolic vulnerability in dopaminergic neurons.

To identify therapeutic agents with potential ASS1-stabilizing capability, we performed virtual docking of 12,316 DrugBank-registered compounds and identified 10 candidates. Among these, S-apomorphine and apomorphine, both non-selective dopaminergic agonists clinically used for the management of motor symptoms in Parkinson’s disease [34, 35], exhibited stable predicted binding to the ASS1 pocket. Demexiptiline, a tricyclic antidepressant used to manage depressive symptoms in Parkinson’s disease [36], and safrazine, a monoamine oxidase inhibitor applied in the treatment of Parkinsonian motor dysfunction[37], similarly exhibited favorable docking profiles. Notably, apomorphine has been reported to attenuate 6-hydroxydopamine–induced apoptotic cell death in SH-SY5Y cells[38]. Our docking results suggest that these clinically used compounds may warrant further evaluation as potential modulators of ASS1-associated metabolic vulnerability.

Propranolol, dexpropranolol, and dichloroisoproterenol—β-adrenergic antagonists—along with tulobuterol, a β2-adrenergic agonist, share core pharmacophores enabling predicted ASS1 occupancy

despite divergent receptor actions. Propranolol, in particular, exhibits antioxidant and cytoprotective effects in cardiomyocytes and endothelial cells and has been reported in clinical trial settings to reduce PD tremor severity [39–41]. Cloridarol, a vasodilatory nitrate, has been shown to inhibit amyloidogenic APP peptides and mitigate cardiomyocyte loss [42]. In addition, TTL, a phenylethanolamine analogue, was identified as a distinct ASS1-binding candidate [43]. Identification of these compounds as ASS1-binding candidates expands their mechanistic interpretability and introduces a translational avenue for dopaminergic neuron preservation, suggesting that modulation of ASS1 activity might be achievable using repurposed agents with established clinical profiles.

Several limitations warrant consideration. First, although our integrative and experimental data tie ASS1 loss to dopaminergic neuron degeneration and elevated ferroptosis susceptibility, more refined mechanistic studies, including rescue experiments and pathway-specific interventions, are required to fully delineate how ASS1 regulates ferroptotic signaling at the molecular level. Second, while our transcriptional stratification framework delineated PD metabolic subclasses, its clinical robustness requires expansion to multicenter cohorts with proteomic and longitudinal follow-up confirmation. Third, the predicted interactions between candidate compounds and ASS1 require further in vitro and in vivo pharmacological validation to determine their functional relevance and potential neuroprotective effects in PD.

In conclusion, this study delineates amino acid metabolic impairment as a defining molecular feature of dopaminergic neuron degeneration in PD, driven centrally by ASS1 suppression. By integrating single-nucleus transcriptomics, bulk expression profiling, and ligand–target prediction, and by providing in vivo and in vitro evidence that ASS1 downregulation promotes ferroptosis-associated neuronal injury, we highlight ASS1 as both a metabolic indicator and a potential therapeutic entry node of dopaminergic vulnerability. These findings establish a framework linking amino acid metabolism to ferroptosis in PD and suggest that targeting ASS1-associated metabolic pathways may represent a potential strategy for preserving dopaminergic neuron viability and modifying disease progression.

4. Methods

4.1 Single-nucleus data acquisition and preprocessing

Single-nucleus RNA-sequencing data of human SNpcs were obtained from the GEO dataset GSE243639 (https://www.ncbi.nlm.nih.gov/geo/) [44]. In the original study, fresh frozen post-mortem midbrain tissue was obtained from the Oregon Brain Bank. The SNpc was identified by H&E staining of 5-μm cryostat sections and neuropathological examination of melanin-containing neurons. H&E-guided 2-mm biopsy punches were then collected for nuclei isolation and single-nucleus RNA sequencing [44].

All preprocessing steps were performed using Seurat (version 4.4.1) [45]. Quality control filtering was executed using the following criteria: 300 ≤ nFeature_RNA ≤ 7,000, nCount_RNA > 1,000 with exclusion of the upper 3% of nCount_RNA values, mitochondrial transcript proportion ≤ 10%, and hemoglobin gene

proportion ≤ 3% (Figure S1). NormalizeData was applied for normalization, 3,000 highly variable features were identified using FindVariableFeatures (vst method), and ScaleData was used for data scaling.

Integration across donors was performed using Seurat's anchor-based integration workflow. PCA was conducted and the first 14 principal components (dims = 1:14) were retained. UMAP embeddings were generated using these components, and clustering was performed with the Leiden algorithm at a resolution of 0.05. Primary cell identities were assigned based on canonical marker genes as follows: neurons (SYT1, SNAP25), astrocytes (AQP4, SLC1A3), microglia (CD74, ITGAM), oligodendrocytes (MBP, MOBP), oligodendrocyte precursor cells (VCAN, PDGFRA), vascular cells (FLT1, DCN), and T cells (THEMIS, CD2) [44]. To better focus on PD-related transcriptional alterations, control-derived nuclei were excluded, and PD donors were stratified into Braak stage I–II and III–IV groups according to the published reference [46].

4.2 Neuronal subset reclustering

Cells annotated as neurons in the first clustering stage were isolated as a separate subset. The neuronal subset was renormalized, highly variable genes were reselected, and expression matrices were rescaled using the same procedures as above. PCA was then performed and the first 23 components (dims = 1:23) were retained. Neuronal reclustering was carried out using the Leiden algorithm with a resolution parameter of 0.3, followed by UMAP visualization. Three neuronal subclusters were identified: dopaminergic neurons characterized by TH, SLC6A3, SNCA and ALDH1A1; excitatory neurons marked by RALGAPA2 and GRIK1; and inhibitory neurons defined by GAD1, GAD2, GABRA1 and GABRB2[44].

4.3 Signature score calculation

Pathway activity at the single-nucleus transcriptomic level was quantified using the irGSEA R package[47]. KEGG pathway gene sets were used as the input gene set collection. Gene set scores were calculated on the RNA assay using normalized expression values, and four algorithms were applied in parallel: AUCell [48], UCell [49], singscore [50] and ssGSEA [51]. For each cell, pathway scores from these four methods were stored in the integrated irGSEA object.

To obtain integrated pathway-level statistics, irGSEA was applied with group-wise comparison based on different cell annotations. Differential pathway enrichment across groups was assessed for all four scoring methods, and Robust Rank Aggregation (RRA) was used to combine results into a consensus significance metric. KEGG pathways with RRA p-values ≤ 0.05 were retained as significantly dysregulated gene sets for downstream visualization and analysis.

4.4 High-dimensional weighted gene co-expression network analysis

High-dimensional weighted gene co-expression network analysis (hdWGCNA v0.4.08) was performed on the neuronal subset using Seurat[52]. Normalized metacell-level expression matrices were used for network construction. Soft-threshold power selection was evaluated, and a power of 7 was applied under

a signed network setting. Gene co-expression modules were identified with a minimum module size of 50 genes and merged at a cut height of 0.2. Module eigengenes were computed, and module connectivity indices were obtained. Module eigengene and hub score distributions were visualized using eigengene projections and module-level UMAP embeddings.

4.5 Differential expression and enrichment analysis of bulk RNA sequencing datasets

Bulk RNA-sequencing data from substantia nigra (GSE20292) were processed using limma [53, 54]. Expression matrices were normalized within the limma framework, and differential expression between PD and control samples was evaluated using linear modeling with empirical Bayes moderation. Differentially expressed genes were defined using $p < 0.05$ and absolute log2 fold-change > 0.3 [55]. Resulting gene rankings were used for Gene Ontology and KEGG pathway enrichment analyses and for GSEA against KEGG reference gene sets using clusterProfiler (v4.12.6) [56].

4.6 ROC discrimination and expression correlation

ROC curves were computed using pROC, and p-values were obtained with Mann-Whitney U test [57]. Pearson correlations were calculated between normalized expression matrices of selected genes. Scatter plots and correlation matrices were used for display.

4.7 Molecular docking

A DrugBank library of 12,316 small molecules was used for virtual screening in the Schrödinger Suite [58, 59]. Molecular properties were calculated with QikProp, and compounds were prefiltered according to Lipinski's rule of five. The crystal structure of human ASS1 (PDB ID: 2NZ2) was prepared using the protein preparation wizard, and the docking grid was defined based on residues reported to interact with the ASS1 agonist LM-2I, including Cys97, Asp182, and Phe68. Ligands were prepared with LigPrep at pH 7.15, and docking was performed sequentially using high-throughput virtual screening (HTVS), standard precision (SP), and extra precision (XP) protocols. Post-docking refinement and binding free energy estimation were conducted using Prime MM-GBSA with the OPLS3 force field [60], and a single representative binding pose was retained for each ligand for downstream analysis and visualization.

4.8 Animal model and tissue collection

Male C57BL/6 mice (8–10 weeks old, 20–25 g) were obtained from an accredited animal facility and maintained under standard laboratory conditions (12 h light/dark cycle, controlled temperature and humidity, with free access to food and water). All experimental procedures were approved by the Institutional Animal Care and Use Committee and performed in accordance with relevant guidelines.

To establish a Parkinson's disease model, mice were administered MPTP (30 mg/kg, intraperitoneal injection) once daily for five consecutive days. Control mice received equivalent volumes of saline. Mice were sacrificed 7 days after the final injection.

For molecular analyses, brains were rapidly dissected on ice, and the substantia nigra region was isolated. Tissues were either snap-frozen in liquid nitrogen for RNA and protein extraction or fixed in 4% paraformaldehyde for histological analysis.

4.9 Cell culture and treatment

SH-SY5Y cell lines (OriCell,Guangzhou,Catalog H8-0101) were cultured under standard culture conditions at 37°C in a humidified atmosphere containing 5% CO2. For the in vitro Parkinson's disease model, cells were treated with MPP^+ at indicated concentrations (0-2500 μM) for 24 h.ASS1 knockdown was achieved by transfecting cells with siRNA targeting ASS1 (siASS1) or negative control siRNA (siNC) using siRNA-Mate Plus transfection reagent (GenePharma, Cat No.G04026) according to the manufacturer's protocol. After 48 h transfection, cells were subjected to MPP^+ treatment for further analyses. Cell viability was assessed using the CCK-8 assay according to standard procedures.

4.10 Quantitative reverse transcription polymerase chain reaction (qRT-PCR)

qRT-PCR was performed as previously described[61]. Total RNA was extracted from substantia nigra tissues using TRIzol reagent according to the manufacturer's instructions. Residual genomic DNA was removed prior to reverse transcription.

cDNA was synthesized from total RNA using a reverse transcription kit, followed by quantitative PCR using TB Green Premix Ex Taq (Takara, Japan). Amplification was carried out under standard cycling conditions, and fluorescence signals were collected at each cycle using a real-time PCR system. The primer sequences were as follows: *ASS1*: forward (5'-GGCTGAAGGAACAAGGCTATGAC-3) and reverse (5'-CCACAAACTCCCTGCTGACATC-3); *β-ACTIN*: forward (5'-CCTGGCACCCAGCACAAT-3) and reverse (5'-GGGCCGGACTCGTCATAC-3). Relative gene expression levels were calculated using the ΔΔCt method, with *β-ACTIN* used as the internal reference gene.

4.11 Western blot analysis

Western blot analysis was conducted performed as previously described [62]. Protein extracts from substantia nigra tissues or SH-SY5Y cells were prepared using RIPA lysis buffer supplemented with protease inhibitors. Protein concentrations were determined using a BCA assay. Equal amounts of protein were separated by SDS-PAGE and transferred onto PVDF membranes. Membranes were blocked with 5% non-fat milk and incubated overnight at 4°C with primary antibodies against ASS1 (Proteintech, Cat No.16210-1-AP), TH (Cell Signaling Technology, #2792), GPX4 (Proteintech, Cat No.67763-1-Ig), and β-actin (Huabio, #et1702-67). After incubation with HRP-conjugated secondary antibodies, protein bands were visualized using an enhanced chemiluminescence (ECL) system. Band intensities were quantified using ImageJ software and normalized to β-actin.

4.12 Immunofluorescence staining

For SH-SY5Y cells, cells were cultured on sterile glass coverslips, fixed with 4% paraformaldehyde for 15 min at room temperature, permeabilized with 0.3% Triton X-100, and blocked with 5% bovine serum albumin. For brain sections, fixed brain tissues were cryoprotected in sucrose, embedded, sectioned at 10–20 μm thickness, permeabilized with 0.3% Triton X-100, and blocked with 5% bovine serum albumin. Samples were then incubated overnight at 4°C with primary antibodies against GPX4 (Proteintech, Cat No. 67763-1-Ig), tyrosine hydroxylase (TH, Cell Signaling Technology, #2792), or ASS1 (Proteintech, Cat No. 16210-1-AP), followed by incubation with appropriate fluorescent secondary antibodies. Nuclei were counterstained with DAPI. Images were captured using a fluorescence microscope, and fluorescence intensity was quantified using ImageJ.

4.13 Detection of lipid peroxidation using BODIPY 581/591 C11

SH-SY5Y cells were cultured in 6-well plates. Lipid peroxidation was assessed using the Lipid Peroxidation Assay Kit with BODIPY™ 581/591 C11 (Beyotime, Cat No. S0043S). Cells were incubated with BODIPY 581/591 C11 at a final concentration of 2 μM in serum-free medium for 30 min at 37°C in the dark. After staining, cells were washed twice with PBS and immediately imaged using a fluorescence microscope (excitation/emission: 488/510 nm for the oxidized form, 581/591 nm for the reduced form). The ratio of fluorescence intensity (oxidized/reduced) was quantified using ImageJ as an indicator of lipid peroxidation levels.

4.14 Statistical analysis

All transcriptomics data processing and statistical analyses were performed in R (version 4.4.1). Data visualization was conducted using ggplot2, pheatmap, irGSEA[47], and clusterProfiler[56]. For transcriptomic comparisons between two groups, the Mann–Whitney U test was used unless otherwise specified. Correlation analyses were performed using Pearson’s correlation coefficients.

All experimental assays were performed with at least three independent biological replicates. Experimental data are presented as mean ± standard deviation (SD). Statistical analyses of experimental data were conducted using GraphPad Prism 10.1.2. Comparisons between two groups were performed using unpaired Student’s t-test, while comparisons among multiple groups were performed using one-way ANOVA followed by appropriate post hoc tests. A p-value < 0.05 was considered statistically significant.

Declarations

Funding

We thank all the participants in this study. This work was supported by Natural Science Foundation of Zhejiang Province (No. LZ25H090004) and Wenzhou High-Level Innovation Team (No. 2024R3002).

Author contributions

Study conception and design: J.M.L., L.P.Z., Z.T.X.; data analysis: L.P.Z., Y.Y.; data acquisition: K.X., Q.Y.L.; animal experiments: C.H.D., Z.T.X.; cell experiments: C.H.D., Z.Y.F.; drafting the manuscript and figures: L.P.Z., Z.T.X.; reviewing the manuscript: J.M.L., J.S., D.C.; funding acquisition: J.S. All authors have read and agreed to the published version of the manuscript.

The authors declare no competing interests.

Data Availability

The transcriptomic datasets analyzed in this study were obtained from the Gene Expression Omnibus (GEO) database, a publicly available repository. Information on small-molecule compounds used for structure-based virtual screening was retrieved from the DrugBank database. All data analyzed in this study are publicly accessible, and the sources are detailed within the Methods section.

References

1. Chemla, A. *et al.*" Parkinson's disease mutant Miro1 causes mitochondrial dysfunction and dopaminergic neuron loss." *Brain* 148, 3607–3622 (2025). https://doi.org/10.1093/brain/awaf051
2. Dionísio, P. A., Amaral, J. D. & Rodrigues, C. M. P." Oxidative stress and regulated cell death in Parkinson's disease." *Ageing Res Rev* 67, 101263 (2021). https://doi.org/10.1016/j.arr.2021.101263
3. Ding, X. S. *et al.*" Ferroptosis in Parkinson's disease: Molecular mechanisms and therapeutic potential." *Ageing Res Rev* 91, 102077 (2023). https://doi.org/10.1016/j.arr.2023.102077
4. Hachiya, Y. *et al.*" Mechanisms of neurodegeneration in neuronal ceroid-lipofuscinoses." *Acta Neuropathol* 111, 168–177 (2006). https://doi.org/10.1007/s00401-005-0024-x
5. Rajapakse, N. W., Nanayakkara, S. & Kaye, D. M." Pathogenesis and treatment of the cardiorenal syndrome: Implications of L-arginine-nitric oxide pathway impairment." *Pharmacol Ther* 154, 1–12 (2015). https://doi.org/10.1016/j.pharmthera.2015.05.011
6. Xiao, Q. *et al.*" Metabolism-dependent ferroptosis promotes mitochondrial dysfunction and inflammation in CD4(+) T lymphocytes in HIV-infected immune non-responders." *EBioMedicine* 86, 104382 (2022). https://doi.org/10.1016/j.ebiom.2022.104382
7. Mattson, M. P. & Magnus, T." Ageing and neuronal vulnerability." *Nat Rev Neurosci* 7, 278–294 (2006). https://doi.org/10.1038/nrn1886
8. Zhu, B. *et al.*" Single-cell transcriptomic and proteomic analysis of Parkinson's disease brains." *Sci Transl Med* 16, eabo1997 (2024). https://doi.org/10.1126/scitranslmed.abo1997
9. Gan, Y. H. *et al.*" Large-scale proteomic analyses of incident Parkinson's disease reveal new pathophysiological insights and potential biomarkers." *Nat Aging* 5, 642–657 (2025). https://doi.org/10.1038/s43587-025-00818-0
10. Vrijsen, S. *et al.*" ATP13A2-mediated endo-lysosomal polyamine export counters mitochondrial oxidative stress." *Proc Natl Acad Sci U S A* 117, 31198–31207 (2020). https://doi.org/10.1073/pnas.1922342117

11. Shen, Y. *et al.*" CSF proteomics identifies early changes in autosomal dominant Alzheimer's disease." *Cell* 187, 6309–6326.e6315 (2024). https://doi.org/10.1016/j.cell.2024.08.049
12. Guo, T. *et al.*" N-homocysteinylation of DJ-1 promotes neurodegeneration in Parkinson's disease." *Aging Cell* 23, e14124 (2024). https://doi.org/10.1111/acel.14124
13. Song, Y., Wu, Z., Xue, H. & Zhao, P." Ferroptosis is involved in regulating perioperative neurocognitive disorders: emerging perspectives." *J Neuroinflammation* 19, 219 (2022). https://doi.org/10.1186/s12974-022-02570-3
14. Du, T. & Han, J." Arginine Metabolism and Its Potential in Treatment of Colorectal Cancer." *Front Cell Dev Biol* 9, 658861 (2021). https://doi.org/10.3389/fcell.2021.658861
15. Morris, S. M., Jr." Regulation of enzymes of the urea cycle and arginine metabolism." *Annu Rev Nutr* 22, 87–105 (2002). https://doi.org/10.1146/annurev.nutr.22.110801.140547
16. Henriet, E. *et al.*" Argininosuccinate synthase 1 (ASS1): A marker of unclassified hepatocellular adenoma and high bleeding risk." *Hepatology* 66, 2016–2028 (2017). https://doi.org/10.1002/hep.29336
17. Hu, Q. *et al.*" ASS1-Mediated Reductive Carboxylation of Cytosolic Glutamine Confers Ferroptosis Resistance in Cancer Cells." *Cancer Res* 83, 1646–1665 (2023). https://doi.org/10.1158/0008-5472.Can-22-1999
18. Lim, L. Q. J. *et al.*" ASS1 metabolically contributes to the nuclear and cytosolic p53-mediated DNA damage response." *Nat Metab* 6, 1294–1309 (2024). https://doi.org/10.1038/s42255-024-01060-5
19. Zou, Z. *et al.*" Naturally-occurring spinosyn A and its derivatives function as argininosuccinate synthase activator and tumor inhibitor." *Nat Commun* 12, 2263 (2021). https://doi.org/10.1038/s41467-021-22235-8
20. Gordon, R. *et al.*" Inflammasome inhibition prevents α-synuclein pathology and dopaminergic neurodegeneration in mice." *Sci Transl Med* 10 (2018). https://doi.org/10.1126/scitranslmed.aah4066
21. Li, X. *et al.*" ROS Regulate Rotenone-induced SH-SY5Y Dopamine Neuron Death Through Ferroptosis-mediated Autophagy and Apoptosis." *Mol Neurobiol* 62, 9271–9289 (2025). https://doi.org/10.1007/s12035-025-04824-6
22. Paul, K. C. *et al.*" Untargeted serum metabolomics reveals novel metabolite associations and disruptions in amino acid and lipid metabolism in Parkinson's disease." *Mol Neurodegener* 18, 100 (2023). https://doi.org/10.1186/s13024-023-00694-5
23. Li, G. *et al.*" Mechanisms of motor symptom improvement by long-term Tai Chi training in Parkinson's disease patients." *Transl Neurodegener* 11, 6 (2022). https://doi.org/10.1186/s40035-022-00280-7
24. Li, H. *et al.*" The potential role of glucose metabolism, lipid metabolism, and amino acid metabolism in the treatment of Parkinson's disease." *CNS Neurosci Ther* 30, e14411 (2024). https://doi.org/10.1111/cns.14411

25. Burki, T. K." Arginine deprivation for ASS1-deficient mesothelioma." *Lancet Oncol* 17, e423 (2016). https://doi.org/10.1016/s1470-2045(16)30446-6
26. Qiu, F. *et al.*" Arginine starvation impairs mitochondrial respiratory function in ASS1-deficient breast cancer cells." *Sci Signal* 7, ra31 (2014). https://doi.org/10.1126/scisignal.2004761
27. Bean, G. R. *et al.*" A metabolic synthetic lethal strategy with arginine deprivation and chloroquine leads to cell death in ASS1-deficient sarcomas." *Cell Death Dis* 7, e2406 (2016). https://doi.org/10.1038/cddis.2016.232
28. Fan, Y. *et al.*" PRMT5-mediated arginine methylation stabilizes GPX4 to suppress ferroptosis in cancer." *Nat Cell Biol* 27, 641–653 (2025). https://doi.org/10.1038/s41556-025-01610-3
29. Dai, H. *et al*." Alterations in immune and antioxidant gene networks by gamma-d-glutamyl-meso-diaminopimelic acid in bovine mammary epithelial cells are attenuated by in vitro supply of methionine and arginine." *J Dairy Sci* 104, 776–785 (2021). https://doi.org/10.3168/jds.2020-19307
30. Liu, Y. *et al.*" A Novel Mutation in Exon 10 of the NOTCH3 Gene in Human Cerebral Microvascular Endothelial Cells Induces CADASIL-Like Pathology and the Therapeutic Effect of Edaravone Dexborneol on Hereditary and Non-hereditary Cerebral Small Vessel Disease." *Neurochem Res* 50, 356 (2025). https://doi.org/10.1007/s11064-025-04596-4
31. Jiang, H. *et al.*" Endothelial cell Ass1 inhibits arteriosclerotic calcification in diabetes mellitus." *Biomed Pharmacother* 181, 117739 (2024). https://doi.org/10.1016/j.biopha.2024.117739
32. Seidl, M. J. *et al.*" ASS1 deficiency is associated with impaired neuronal differentiation in zebrafish larvae." *Mol Genet Metab* 141, 108097 (2024). https://doi.org/10.1016/j.ymgme.2023.108097
33. Cao, X. *et al.*" Role of Argininosuccinate Synthase 1 -Dependent L-Arginine Biosynthesis in the Protective Effect of Endothelial Sirtuin 3 Against Atherosclerosis." *Adv Sci (Weinh)* 11, e2307256 (2024). https://doi.org/10.1002/advs.202307256
34. Sam, E. E. & Verbeke, N." Free radical scavenging properties of apomorphine enantiomers and dopamine: possible implication in their mechanism of action in parkinsonism." *J Neural Transm Park Dis Dement Sect* 10, 115–127 (1995). https://doi.org/10.1007/bf02251227
35. Zaleska, B. & Domzał, T." [Apomorphine in treatment of Parkinson's disease with fluctuations]." *Neurol Neurochir Pol* 33, 1297–1303 (1999).
36. Angelopoulou, E. *et al.*" Pharmacological and Non-Pharmacological Treatments for Depression in Parkinson's Disease: An Updated Review." *Medicina (Kaunas)* 59 (2023). https://doi.org/10.3390/medicina59081454
37. Yokoyama, T., Karube, T. & Iwata, N." Comparative studies of the effects of RS-8359 and safrazine on monoamine oxidase in-vitro and in-vivo in mouse brain." *J Pharm Pharmacol* 41, 32–36 (1989). https://doi.org/10.1111/j.2042-7158.1989.tb06324.x
38. Hara, H., Ohta, M., Ohta, K., Kuno, S. & Adachi, T." Apomorphine attenuates 6-hydroxydopamine-induced apoptotic cell death in SH-SY5Y cells." *Redox Rep* 8, 193–197 (2003). https://doi.org/10.1179/135100003225002682

39. Mak, I. T. & Weglicki, W. B." Comparative antioxidant activities of propranolol, nifedipine, verapamil, and diltiazem against sarcolemmal membrane lipid peroxidation." *Circ Res* 66, 1449–1452 (1990). https://doi.org/10.1161/01.res.66.5.1449
40. Dickens, B. F., Weglicki, W. B., Boehme, P. A. & Mak, T. I." Antioxidant and lysosomotropic properties of acridine-propranolol: protection against oxidative endothelial cell injury." *J Mol Cell Cardiol* 34, 129–137 (2002). https://doi.org/10.1006/jmcc.2001.1495
41. van der Heide, A. *et al.*" Propranolol Reduces Parkinson's Tremor and Inhibits Tremor-Related Activity in the Motor Cortex: A Placebo-Controlled Crossover Trial." *Ann Neurol* 97, 741–752 (2025). https://doi.org/10.1002/ana.27159
42. Tang, Y. *et al.*" Repurposing a Cardiovascular Disease Drug of Cloridarol as hIAPP Inhibitor." *ACS Chem Neurosci* 12, 1419–1427 (2021). https://doi.org/10.1021/acschemneuro.1c00091
43. Gee, C. L. *et al.*" Mode of binding of methyl acceptor substrates to the adrenaline-synthesizing enzyme phenylethanolamine N-methyltransferase: implications for catalysis." *Biochemistry* 44, 16875–16885 (2005). https://doi.org/10.1021/bi051636b
44. Martirosyan, A. *et al.*" Unravelling cell type-specific responses to Parkinson's Disease at single cell resolution." *Mol Neurodegener* 19, 7 (2024). https://doi.org/10.1186/s13024-023-00699-0
45. Satija, R., Farrell, J. A., Gennert, D., Schier, A. F. & Regev, A." Spatial reconstruction of single-cell gene expression data." *Nat Biotechnol* 33, 495–502 (2015). https://doi.org/10.1038/nbt.3192
46. Ding, Z. T. *et al.*" Characteristics of alpha-synucleinopathy in centenarians." *Acta Neuropathol* 111, 450–458 (2006). https://doi.org/10.1007/s00401-005-0015-y
47. Fan, C. *et al.*" irGSEA: the integration of single-cell rank-based gene set enrichment analysis." *Brief Bioinform* 25 (2024). https://doi.org/10.1093/bib/bbae243
48. Liu, Y. *et al.*" Integrated bulk and single-cell transcriptomes reveal pyroptotic signature in prognosis and therapeutic options of hepatocellular carcinoma by combining deep learning." *Brief Bioinform* 25 (2023). https://doi.org/10.1093/bib/bbad487
49. Andreatta, M. & Carmona, S. J." UCell: Robust and scalable single-cell gene signature scoring." *Comput Struct Biotechnol J* 19, 3796–3798 (2021). https://doi.org/10.1016/j.csbj.2021.06.043
50. Mao, Y. *et al.*" Cross-platform comparison of immune signatures in immunotherapy-treated patients with advanced melanoma using a rank-based scoring approach." *J Transl Med* 21, 257 (2023). https://doi.org/10.1186/s12967-023-04092-9
51. Jin, Y. *et al.*" Identification of novel subtypes based on ssGSEA in immune-related prognostic signature for tongue squamous cell carcinoma." *Cancer Med* 10, 8693–8707 (2021). https://doi.org/10.1002/cam4.4341
52. Morabito, S., Reese, F., Rahimzadeh, N., Miyoshi, E. & Swarup, V." hdWGCNA identifies co-expression networks in high-dimensional transcriptomics data." *Cell Rep Methods* 3, 100498 (2023). https://doi.org/10.1016/j.crmeth.2023.100498
53. Zhang, Y., James, M., Middleton, F. A. & Davis, R. L." Transcriptional analysis of multiple brain regions in Parkinson's disease supports the involvement of specific protein processing, energy metabolism,

and signaling pathways, and suggests novel disease mechanisms." *Am J Med Genet B Neuropsychiatr Genet* 137b, 5–16 (2005). https://doi.org/10.1002/ajmg.b.30195

54. Law, C. W., Chen, Y., Shi, W. & Smyth, G. K." voom: Precision weights unlock linear model analysis tools for RNA-seq read counts." *Genome Biol* 15, R29 (2014). https://doi.org/10.1186/gb-2014-15-2-r29
55. Knorr, S. *et al.*" Epigenetic and transcriptomic alterations in offspring born to women with type 1 diabetes (the EPICOM study)." *BMC Med* 20, 338 (2022). https://doi.org/10.1186/s12916-022-02514-x
56. Wu, T. *et al.*" clusterProfiler 4.0: A universal enrichment tool for interpreting omics data." *Innovation (Camb)* 2, 100141 (2021). https://doi.org/10.1016/j.xinn.2021.100141
57. Carpenter, J. & Bithell, J." Bootstrap confidence intervals: when, which, what? A practical guide for medical statisticians." *Stat Med* 19, 1141–1164 (2000). https://doi.org/10.1002/(sici)1097-0258(20000515)19:9%3C1141::aid-sim479%3E3.0.co;2-f
58. Knox, C. *et al.*" DrugBank 6.0: the DrugBank Knowledgebase for 2024." *Nucleic Acids Res* 52, D1265-d1275 (2024). https://doi.org/10.1093/nar/gkad976
59. Friesner, R. A. *et al.*" Glide: a new approach for rapid, accurate docking and scoring. 1. Method and assessment of docking accuracy." *J Med Chem* 47, 1739–1749 (2004). https://doi.org/10.1021/jm0306430
60. Lyne, P. D., Lamb, M. L. & Saeh, J. C." Accurate prediction of the relative potencies of members of a series of kinase inhibitors using molecular docking and MM-GBSA scoring." *J Med Chem* 49, 4805–4808 (2006). https://doi.org/10.1021/jm060522a
61. Liang, F. *et al.*" Biomass fuel induces neuroinflammation and neurodegeneration via the astrocyte-microglia IL-17A/IL-17RA pathway." *J Hazard Mater* 494, 138569 (2025). https://doi.org/10.1016/j.jhazmat.2025.138569
62. Xu, Z. *et al.*" Elevated blood microplastics and their potential association with Parkinson's disease." *J Hazard Mater* 500, 140431 (2025). https://doi.org/10.1016/j.jhazmat.2025.140431

Figures

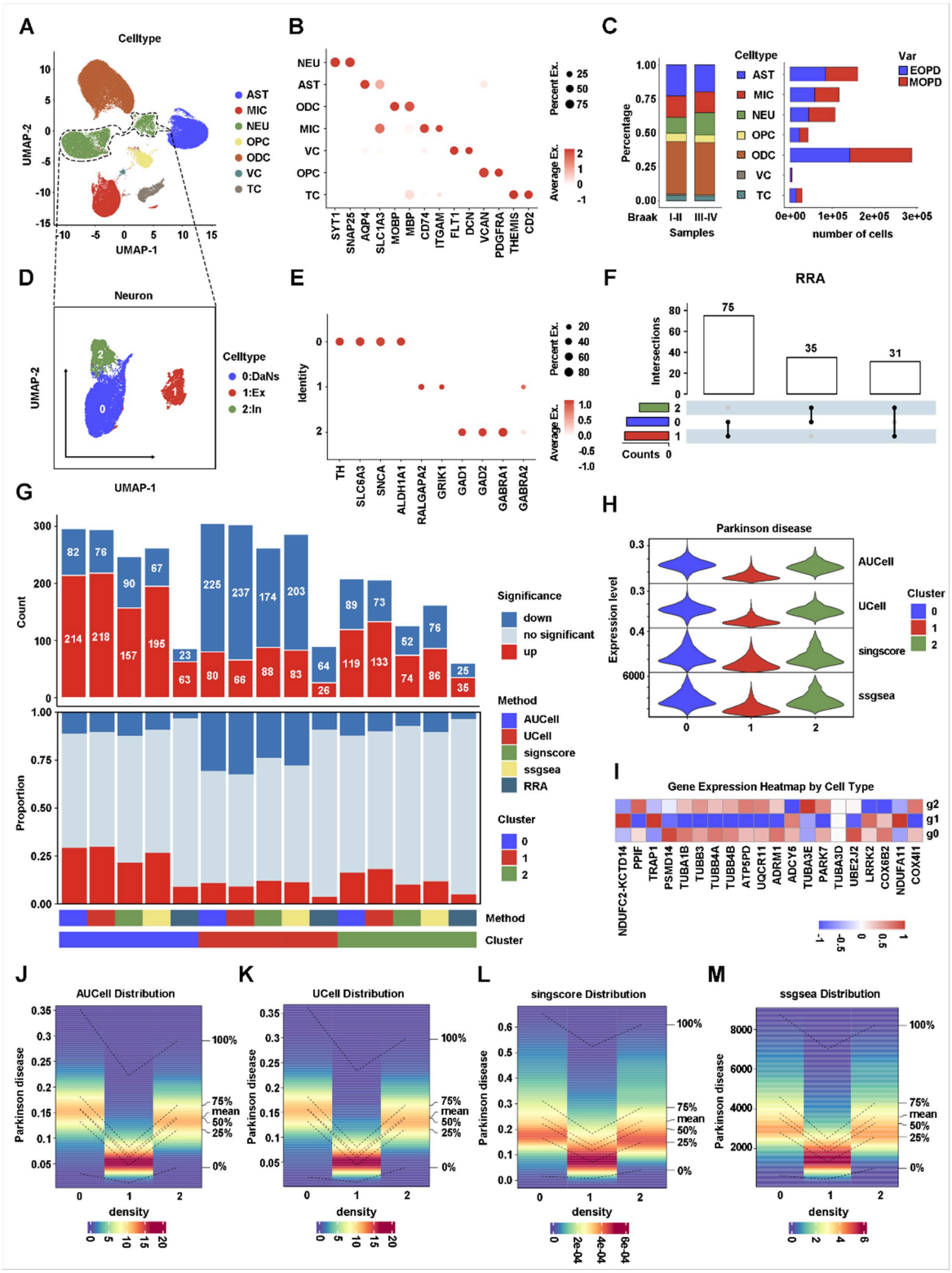


Figure 1

Single-cell landscape of human SNpc and identification of dopaminergic neurons. (A) UMAP visualization of integrated single-cell data showing major brain cell types, including neurons (NEU), astrocytes (AST), oligodendrocytes (ODC), microglia (MIC), vascular cells (VC), oligodendrocyte precursor cells (OPC) and T cells (TC). (B) Dot plot of canonical marker genes used to annotate each major cell type. (C) Stacked bar plots showing the relative proportions of major cell types across Braak

stage I-II and Braak stage III-IV Parkinson's disease samples. (D) UMAP of reclustered neurons indicating three neuronal subtypes, including dopaminergic neurons (DaNs), excitatory neurons (Ex) and inhibitory neurons (In). (E) Dot plot of neuronal markers confirming cluster 0 as dopaminergic neurons, cluster 1 as excitatory neurons and cluster 2 as inhibitory neurons. (F) UpSet plot showing overlaps of significantly dysregulated KEGG pathways among the three neuronal subtypes based on RRA-integrated irGSEA scores. (G) Stacked bar plots summarizing numbers and proportions of upregulated and downregulated pathways in each neuronal subtype and for each scoring method. (H) Violin plots of Parkinson's disease pathway scores across neuronal subtypes for the four scoring algorithms. (I) Heatmap of Parkinson's disease pathway genes across neuronal subtypes. (J–M) Density and ridgeline plots of Parkinson's disease pathway scores for each scoring method, highlighting higher scores in dopaminergic neurons.

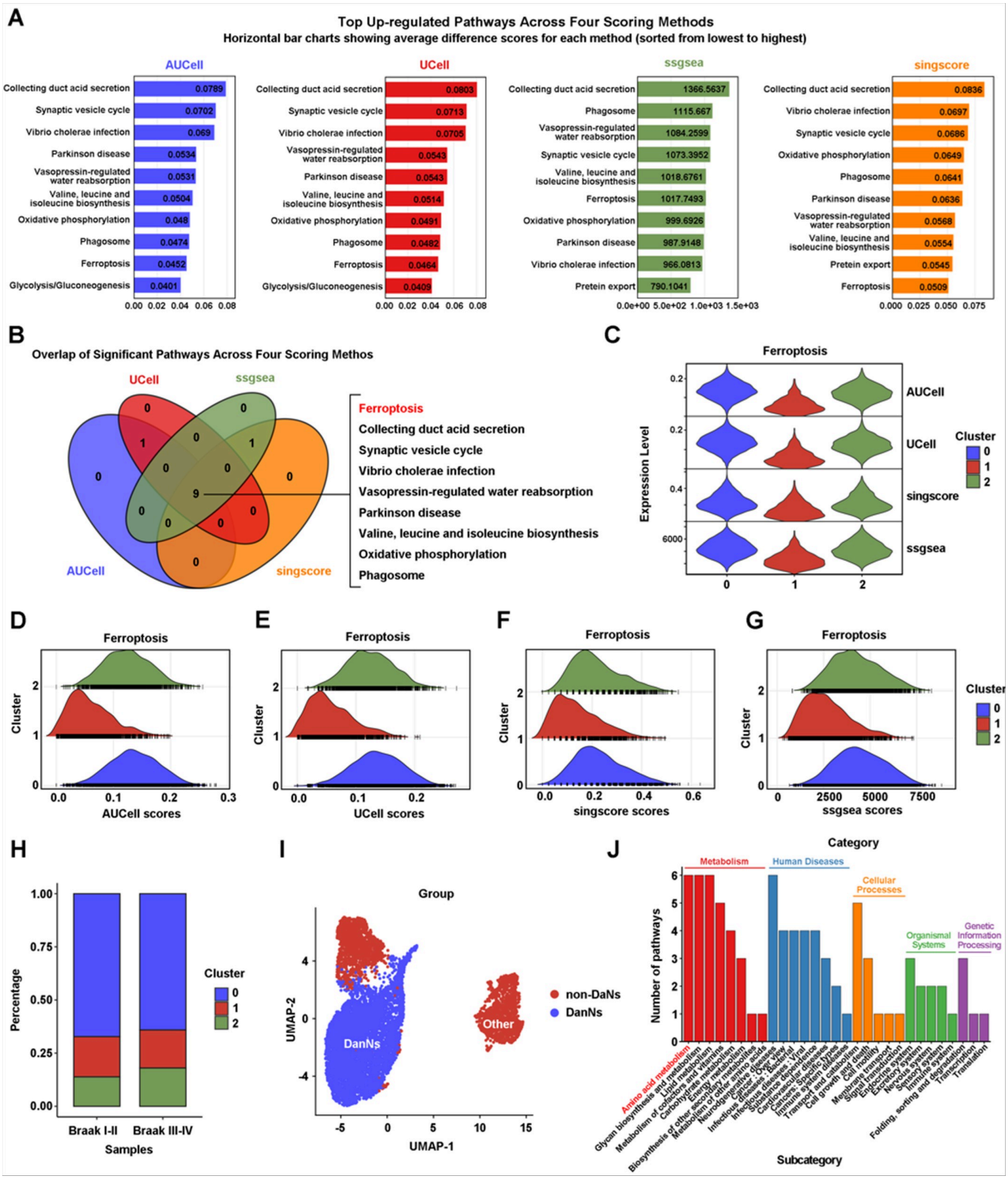


Figure 2

Ferroptosis signatures in neuronal subtypes and emphasis on amino acid metabolism. (A) Top-ranked KEGG pathways in dopaminergic neurons (cluster 0) based on average difference scores across four irGSEA methods (AUCell, UCell, ssGSEA, and singscore). (B) Venn diagram showing overlap of significantly enriched pathways across the four scoring methods, identifying nine shared pathways including ferroptosis. (C) Violin plots showing ferroptosis pathway scores across neuronal subtypes

under four scoring methods. (D–G) Density/ridge plots showing the distribution of ferroptosis pathway scores across neuronal subtypes for each scoring method. (H) Stacked bar plots showing the relative proportions of neuronal subtypes across Braak stage I–II and III–IV samples. (I) UMAP visualization distinguishing dopaminergic neurons (DaNs) and non-dopaminergic neurons (non-DaNs). (J) Bar plot summarizing significantly altered KEGG pathway categories and subcategories, highlighting metabolism as the dominant category and amino acid metabolism as the most enriched subcategory in dopaminergic neurons.

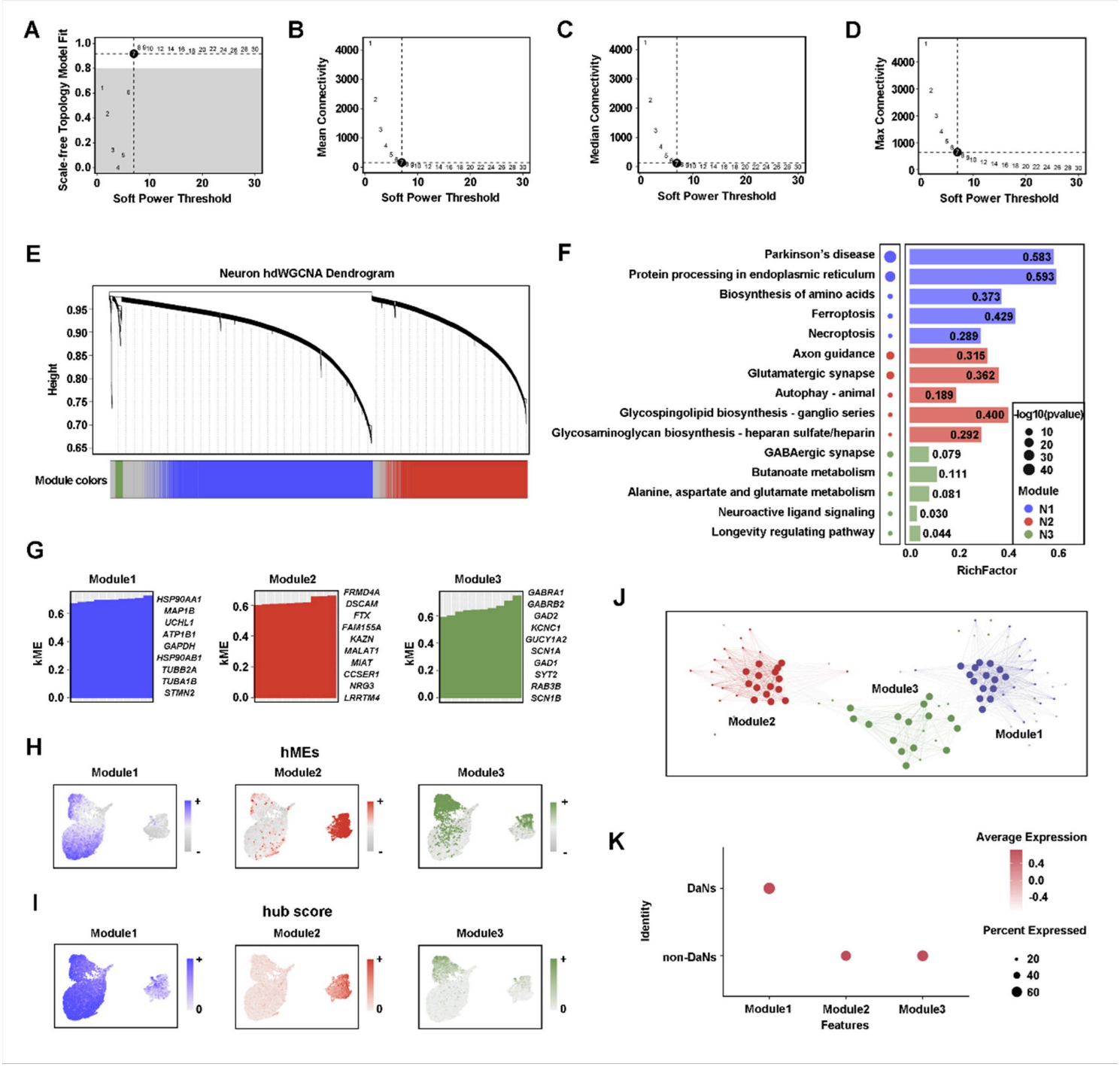


Figure 3

Neuron-specific hdWGCNA modules and their distribution across neuronal subtypes. (A–D) Plots of scale-free topology fit, mean connectivity, median connectivity and maximum connectivity as a function of soft-threshold power, with power 7 selected. (E) Gene dendrogram with modules indicated by distinct colors, showing three major modules. (F) KEGG enrichment results for each module shown as a bar plot. (G) Bar plots of the top ten hub genes in each module ranked by eigengene connectivity. (H) UMAP projections of module eigengene (hME) scores. (I) UMAP projections of hub scores for the modules. (J) Network plot showing the top 30 hub genes per module and their connections. (K) Dot plot comparing average module expression between dopaminergic and non-dopaminergic neurons.

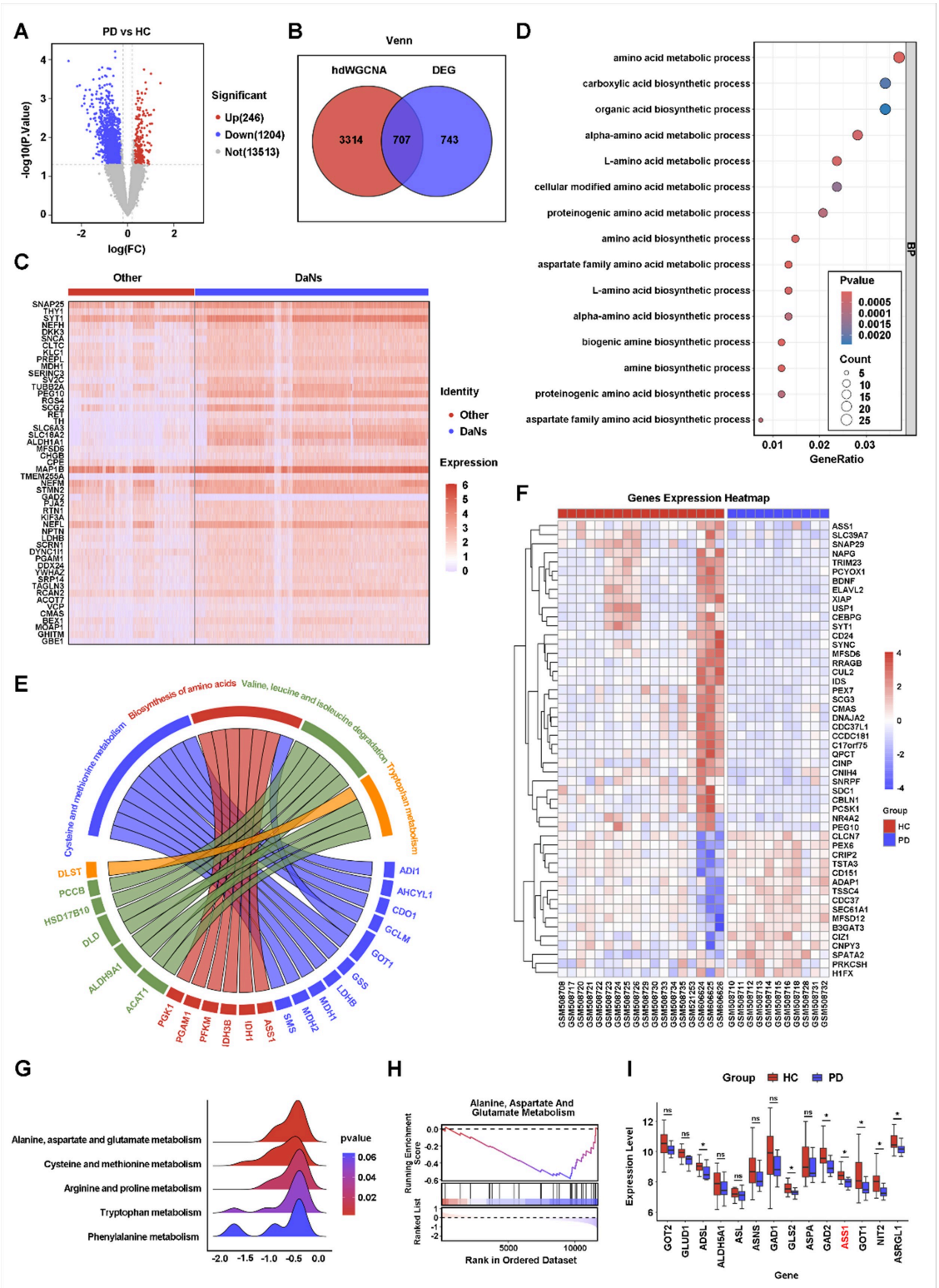


Figure 4

Bulk RNA-seq integration reveals amino acid metabolic reprogramming and downregulation of amino acid metabolism genes in PD. (A) Volcano plot of bulk differentially expressed genes between PD and control substantia nigra. (B) Venn diagram showing the overlap between neuron hdWGCNA module genes and bulk differentially expressed genes. (C) Heatmap of 50 overlapping genes in the single-cell dataset across dopaminergic and other neurons. (D) GO biological process enrichment of overlapping

genes emphasizing amino acid metabolism–related processes. (E) KEGG chord diagram linking overlapping genes to amino acid metabolism pathways. (F) Heatmap of the same 50 genes in the bulk dataset across control and PD samples. (G) Ridgeline plot summarizing GSEA normalized enrichment scores for selected amino acid metabolism pathways. (H) GSEA enrichment plot for the “Alanine, aspartate and glutamate metabolism” pathway. (I) Boxplots showing expression of 14 representative genes from this pathway in control versus PD bulk samples.

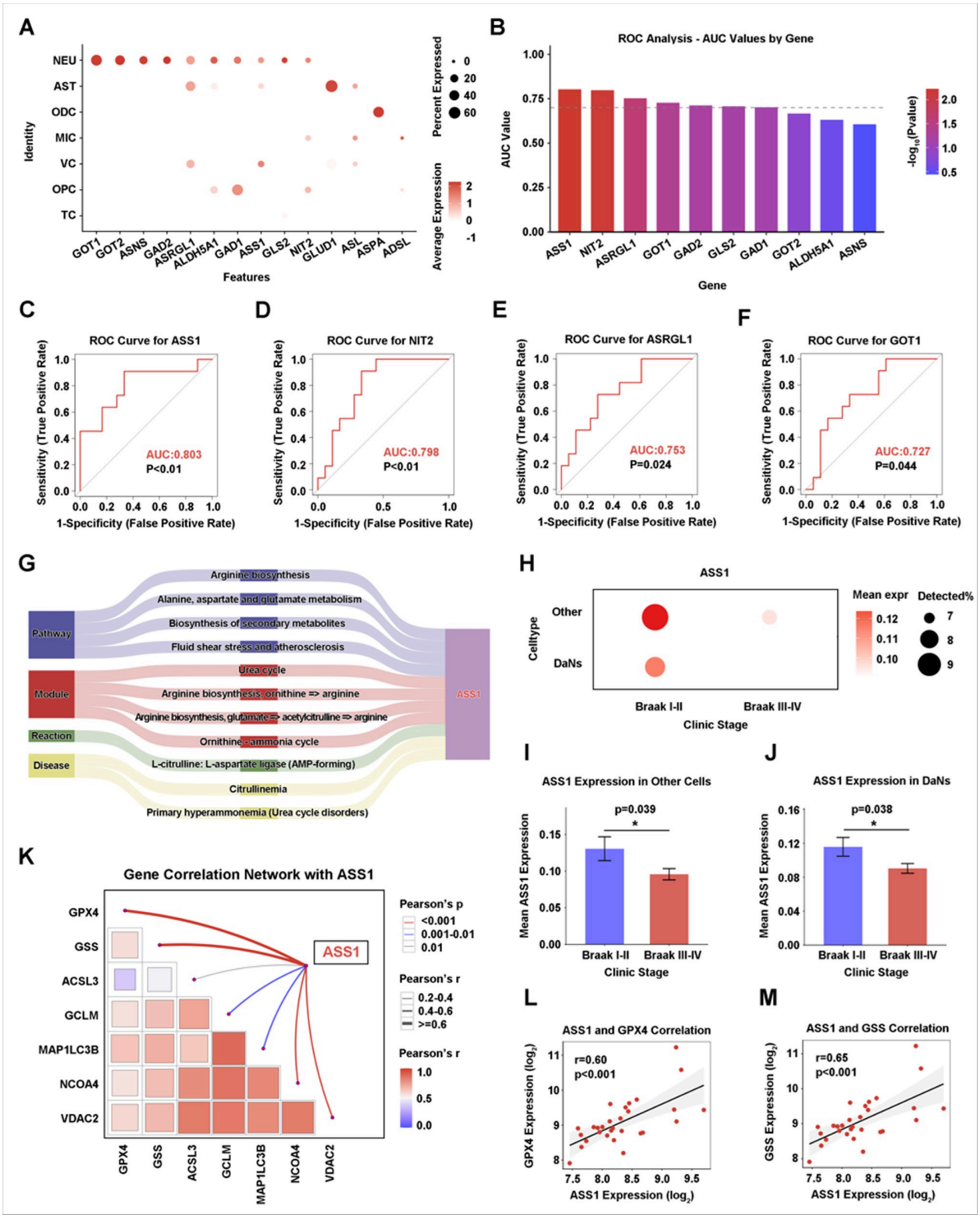


Figure 5

ASS1 is a key metabolic gene associated with ferroptosis-related signatures in Parkinson's disease. (A) Dot plot showing expression of 14 pathway genes across major brain cell types in the single-cell dataset. (B) Bar plot of AUC values from ROC analysis for the 10 neuron-expressed genes, highlighting ASS1 with the highest AUC (0.803). (C–F) ROC curves for ASS1, NIT2, ASRGL1 and GOT1 in distinguishing PD from control samples. (G) Sankey diagram summarizing KEGG pathways and reactions associated with ASS1. (H) Dot plot showing ASS1 expression across neuronal subtypes and Braak stages (I-II vs III-IV) in the single-nucleus dataset. (I-J) Differential expression analysis of ASS1 between dopaminergic and non-dopaminergic neurons across Braak stages. (K) Correlation matrix or network showing genes strongly correlated with ASS1, including GPX4 and GSS. (L-M) Scatterplots depicting the positive correlations between ASS1 and GPX4 and GSS.

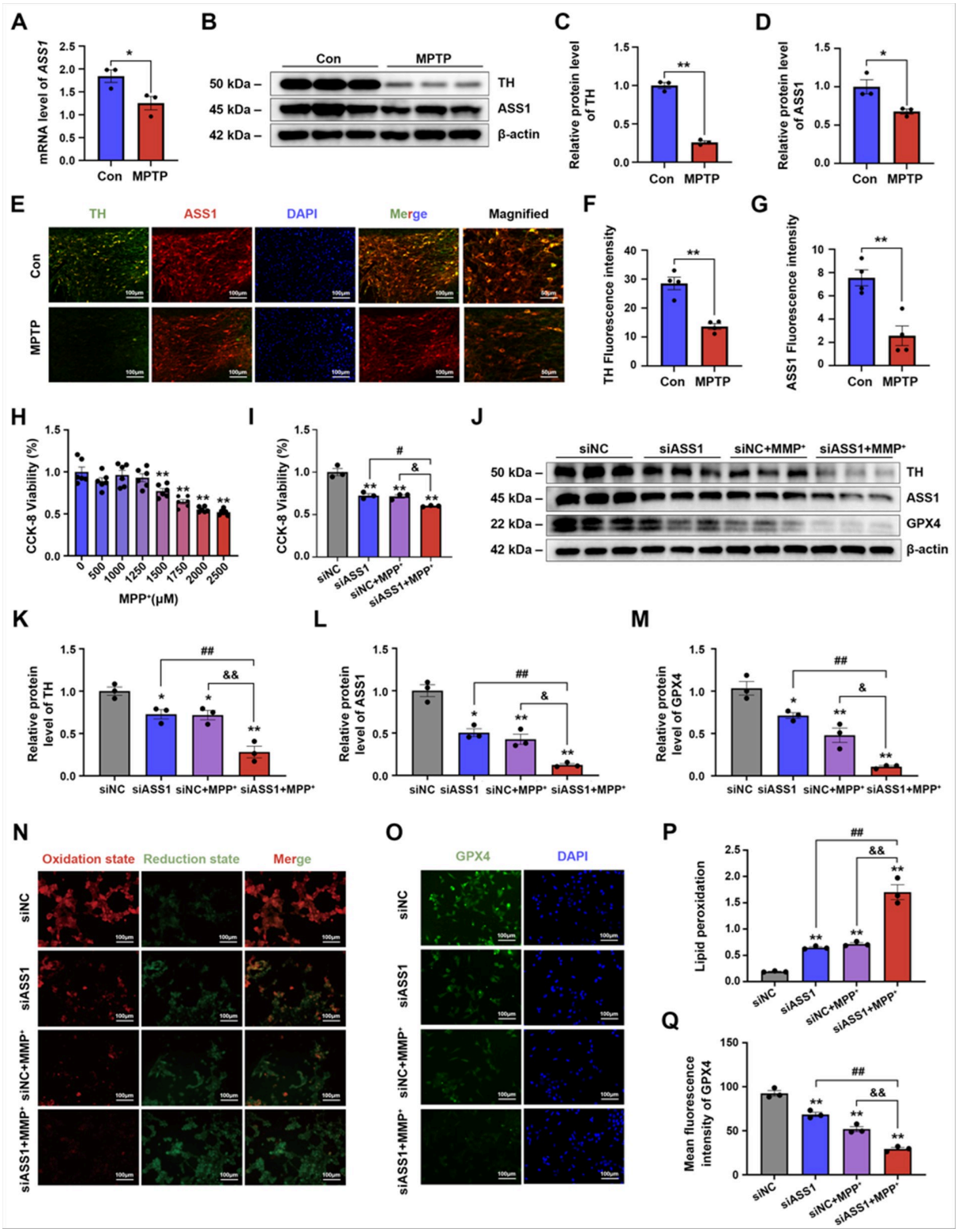


Figure 6

ASS1 downregulation promotes ferroptosis and dopaminergic neuronal injury in PD models. (A) Relative mRNA expression of ASS1 in the substantia nigra of control and MPTP-treated mice determined by qPCR. (B) Representative western blot images showing TH and ASS1 protein levels in control and MPTP groups. (C–D) Quantification of TH and ASS1 protein expression normalized to β-actin. (E) Immunofluorescence staining of TH (green), ASS1 (red), and DAPI (blue) in the substantia nigra of

control and MPTP-treated mice, with merged and magnified views. (F–G) Quantification of TH-positive fluorescence intensity and ASS1 fluorescence intensity. (H) CCK-8 assay showing dose-dependent effects of MPP^+ on SH-SY5Y cell viability. (I) Cell viability of SH-SY5Y cells under different conditions: siNC, siASS1, siNC+MPP^+, and siASS1+MPP^+. (J) Representative western blot images of TH, ASS1, and GPX4 in SH-SY5Y cells across experimental groups. (K–M) Quantification of TH, ASS1, and GPX4 (M) protein levels normalized to β-actin. (N) C11-BODIPY staining showing lipid peroxidation (oxidized/red, reduced/green) in SH-SY5Y cells under indicated conditions. (O) Immunofluorescence staining of GPX4 (green) with DAPI (blue). (P) Quantification of lipid peroxidation levels based on C11-BODIPY staining. (Q) Quantification of GPX4 fluorescence intensity.

Supplementary Files

This is a list of supplementary files associated with this preprint. Click to download.

- RawWesternblotimages.pdf
- FigureS1toS4.docx